NAVAL POSTGRADUATE SCHOOL
Monterey, California

THESIS

AMPLITUDE MODULATION USING A NONLINEAR OPTICAL LOOP MIRROR

by

David S. Grennek

December 1998

Thesis Advisor: Andrés Larraza
Co-Advisor: H. Sarma Lakkaraju

Approved for public release; distribution is unlimited.

REPORT DOCUMENTATION PAGE

Form Approved
OMB No. 0704-0188

1. AGENCY USE ONLY *(Leave blank)*	2. REPORT DATE	3. REPORT TYPE AND DATES COVERED
	December 1998	Master's Thesis

4. TITLE AND SUBTITLE
AMPLITUDE MODULATION USING A NONLINEAR OPTICAL LOOP MIRROR

5. FUNDING NUMBERS

6. AUTHOR(S)
Grennek, David S.

7. PERFORMING ORGANIZATION NAME(S) AND ADDRESS(ES)
Naval Postgraduate School
Monterey, CA 93943-5000

8. PERFORMING ORGANIZATION REPORT NUMBER

9. SPONSORING / MONITORING AGENCY NAME(S) AND ADDRESS(ES)

10. SPONSORING/MONITORING AGENCY REPORT NUMBER

11. SUPPLEMENTARY NOTES
The views expressed in this thesis are those of the author and do not reflect the official policy or position of the Department of Defense or the U.S. Government.

12a. DISTRIBUTION / AVAILABILITY STATEMENT
Approved for public release; distribution is unlimited.

12b. DISTRIBUTION CODE

13. ABSTRACT *(Maximum 200 words)*

The nonlinear optical loop mirror (NOLM) configuration has been studied extensively within the context of pulsed and/or quasi-CW laser sources. As such, the NOLM holds great promise in the areas of soliton switching, pulse compression and high data rate communications. However, comparatively little research has been done with CW sources. In this investigation, the theoretical properties of the NOLM are explored experimentally with the aid of a CW Nd:YAG laser operating in the infrared region. Specifically, the nonlinear effects of self-phase modulation are characterized. For a beam of sufficient intensity, its optical path through the fiber may be altered due to the dependence of the phase on intensity. Thus, two coherent beams of light of differing intensity can be made to interfere constructively or destructively even though the physical paths are identical. In the NOLM configuration, the potential result is an amplitude modulated output beam exhibiting a repetition rate several orders of magnitude greater than that of the input. Two dissimilar single-mode fibers as well as two custom-built fixed-ratio asymmetric fiberoptic couplers are utilized in the experiment. Correlation with theory is emphasized and follow-on projects are discussed.

14. SUBJECT TERMS
Fiberoptics, Nd:YAG Laser, Nonlinear Index of Refraction, Self-phase Modulation

15. NUMBER OF PAGES
58

16. PRICE CODE

17. SECURITY CLASSIFICATION OF REPORT	18. SECURITY CLASSIFICATION OF THIS PAGE	19. SECURITY CLASSIFICATION OF ABSTRACT	20. LIMITATION OF ABSTRACT
Unclassified	Unclassified	Unclassified	UL

NSN 7540-01-280-5500

Standard Form 298 (Rev. 2-89)
Prescribed by ANSI Std 239-18

Approved for public release; distribution is unlimited

AMPLITUDE MODULATION USING A NONLINEAR OPTICAL LOOP MIRROR

David S. Grennek
Lieutenant, United States Navy
B.S., United States Naval Academy, 1989

Submitted in partial fulfillment of the
requirements for the degree of

MASTER OF SCIENCE IN APPLIED PHYSICS

from the

NAVAL POSTGRADUATE SCHOOL
December 1998

Author: _____
David S. Grennek

Approved by: _____
Andrés Larraza, Thesis Advisor

_____
H. Sarma Lakkaraju, Co-Advisor

_____
William B. Maier II, Chairman
Department of Physics

ABSTRACT

The nonlinear optical loop mirror (NOLM) configuration has been studied extensively within the context of pulsed and/or quasi-CW laser sources. As such, the NOLM holds great promise in the areas of soliton switching, pulse compression and high data rate communications. However, comparatively little research has been done with CW sources. In this investigation, the theoretical properties of the NOLM are explored experimentally with the aid of a CW Nd:YAG laser operating in the infrared region. Specifically, the nonlinear effects of self-phase modulation are characterized. For a beam of sufficient intensity, its optical path through the fiber may be altered due to the dependence of the phase on intensity. Thus, two coherent beams of light of differing intensity can be made to interfere constructively or destructively even though the physical paths are identical. In the NOLM configuration, the potential result is an amplitude modulated output beam exhibiting a repetition rate several orders of magnitude greater than that of the input. Two dissimilar single-mode fibers as well as two custom-built fixed-ratio asymmetric fiberoptic couplers are utilized in the experiment. Correlation with theory is emphasized and follow-on projects are discussed.

TABLE OF CONTENTS

ACKNOWLEDGEMENT

First and foremost, I thank my family for their unending support over the last two and one-half years. I recognize the many sacrifices that they have made on my behalf while I struggled with being a student again. None of my accomplishments would have been possible without their constant words of encouragement.

Secondly, I thank my thesis advisors, Dr. Andrés Larraza of the Naval Postgraduate School and Dr. H. Sarma Lakkaraju of San José State University. Needless to say, I learned a tremendous amount from both individuals. Without their guidance and dedicated oversight, this thesis would have never gotten off the ground.

Lastly, I extend a heartfelt thank-you to both David J. DiGiovanni of Lucent Technologies and Frederic Quan of Corning Incorporated for their gracious donation of both fiberoptic materials and information vital to this investigation. I am confident that future generations of Physics department thesis students will echo my sentiments.

I. INTRODUCTION

A. BACKGROUND

The field of fiberoptics has blossomed over the last several years. With the advent of the 'information age', the public has demanded not only more reliable but also faster means of communication. With an operating frequency in the neighborhood of one petahertz (PHz = 10^{15} Hz), the bandwidth offered by fiber is virtually unlimited (by today's standards). Consequently, 'glass' is rapidly replacing copper as the medium of choice in everything from local area networks (LANs) to cable television installations to transatlantic telephone lines.

Historically, signal attenuation due to fiber impurities had been a major obstacle in the growth curve of the fiber industry. Continuous improvements in manufacturing processes, however, have mitigated this as a serious concern; fiber spans of hundreds of kilometers or more are now commonplace in our society. With appropriate choice of operating wavelength, attenuation is on the order of only a small fraction of a decibel per kilometer.

The move toward a fiber world does not come without difficulties, though. As data rates and fiber spans are pushed toward ever-greater heights, new bumps in the road to progress continue to present themselves. Nonlinearity is one such hurdle that must be cleared if we hope to sustain the current growth rate of technological evolution. The combination of higher optical powers and longer fiber lengths dictates that nonlinearities can no longer be ignored. As a result, a tremendous volume of research has been and continues to be conducted in the field of nonlinear optics. In the study of fiberoptics, one of the most intriguing concepts to be introduced in the last ten years is that of the Nonlinear Optical Loop Mirror or NOLM for short. The NOLM design actively exploits the inherent nonlinearities in the fiber to achieve quantifiable performance gains. Variants of the NOLM are finding applications in everything from communication systems to electro-optic sensors.

B. MOTIVATION

Fiberoptics is clearly at the forefront of the ongoing technological revolution sweeping this country and the rest of the world. Optical computing and processing is quickly becoming a reality. However, with such a rapid growth rate, it is challenging to stay abreast of the latest trends in the field. New discoveries take place every day, literally; in contrast, groundbreaking findings occur much less frequently. As the theory of the NOLM was, in itself, somewhat of a revolutionary concept when it was first proposed in 1988, we will provide an independent derivation of the theory and an experimental investigation of the basic design.

In the past, much of the fiberoptic research treated the fiber merely as an 'information pipe', a means of conveying bits of digital information from one location to another. The emphasis was on the components at either end of the fiber and not on the fiber itself. However, to truly capitalize on the inherent capabilities of the fiber, we must investigate the physics underlying the complex propagation characteristics that we observe. Accordingly, the nonlinearities of the system play a critical role. In particular, the concept of the nonlinear index of refraction and its corresponding intensity dependence are fundamental to the study of fiberoptics. By exploiting the principle of self-phase modulation (SPM), the NOLM configuration is finding applications in mode locking of lasers, electro-optic amplitude modulation, laser tunability and soliton pulse propagation. Thus, investigation of the NOLM provides an appropriate initiation into the vast world of nonlinear fiberoptics. Moreover, this research should serve adequately as a starting point for future experimental work in the field of nonlinear fiberoptics at the Naval Postgraduate School.

For this investigation, we will be concentrating on the electro-optic modulation enhancement characteristics of the NOLM. Specifically, our two primary objectives are as follows: 1) to derive independently the various equations applicable to the process of self-phase modulation in the context of the NOLM and 2) experimentally verify the validity of the theory in the lab. To achieve our second objective, we will be utilizing a Nd:YAG laser acting as the input source to two NOLMs of dissimilar configuration.

Input and output powers will be measured and the data plotted; it is anticipated that the resultant curves derived from the experimental data will correlate favorably with the theoretical predictions.

C. SCOPE OF THIS THESIS

The structure of this thesis is as follows: In Chapter II we introduce some of the basic optic and fiberoptic principles that are necessary to sufficiently explain the more advanced nonlinear concepts. This leads directly into an abbreviated review of the theory of nonlinear optics, specifically the nonlinear index of refraction and SPM as they relate to fiber. Chapter II concludes with a detailed physical description of the NOLM and a thorough development of the principles essential to its operation. Chapter III consists of two main sections. The first section of the chapter specifies the various pieces of gear utilized in the experiment. This includes the specifications for both the test equipment as well as the capabilities of the fiber spools and couplers to be used in the course of the investigation. The latter part of Chapter III elaborates on the actual equipment setup and testing procedures. Finally, Chapter IV will summarize the experimental results, present conclusions and provide recommendations on potential future experimental efforts utilizing the NOLM configuration. Again, the ultimate goal is to experimentally demonstrate the validity of the NOLM design and associated theory.

II. FIBEROPTICS AND THE OPTICAL LOOP MIRROR

A. BASIC OPTICS AND FIBEROPTICS

The concept of transmitting information using guided light has been around for more than 100 years. Moreover, the utilization of waveguides fabricated of glass or plastic has existed for more than a quarter of a century. Not surprisingly, the field of fiberoptics has experienced tremendous growth in the last several years: from fiber-optic communications, to medical applications using optical fibers. In this section, we will discuss some of the basic underlying principles of fiberoptics, with emphasis on the concepts and terms specifically related to our experimental investigation.

1. Light in Materials

The speed of propagation of light in a vacuum is the well-known constant, c, where c is approximately 3×10^8 meters per second. In contrast, the speed of propagation of light in matter is dependent upon the material and is always less than c. The quantity that relates the two speeds is known as the index of refraction, n, of the material. In terms of n, the speed of propagation v in a material is $v = c / n$. Thus, the value of n is always greater than 1.0. For water, n is about 1.33; for glass, it is typically around 1.5. The speed of propagation, v, depends also on the frequency of the incident light. Ignoring any nonlinearities, the refractive index is therefore a function of the frequency (or equivalently, the wavelength) as well. To a considerable degree of accuracy, the refractive index, n, may be expressed by the Sellmeier equation (Agrawal, 1995).

$$n^2(\omega) = 1 + \sum_{j=1}^{3} \frac{B_j \omega_j^2}{\omega_j^2 - \omega^2} \qquad (2.1)$$

where the B_j and ω_j terms are empirically determined for the individual material. Shown in Figure 2.1 is a graphical representation of Equation (2.1). This effect is known as

chromatic dispersion and it is a manifestation of each material's characteristic resonance frequencies ω_j.

For optical fibers, dispersive effects can be either normal or anomalous, with the transition wavelength at approximately 1.3 μm. At shorter wavelengths, dispersion is normal with high frequencies traveling slower than low frequencies. In contrast, the reverse is true in the anomalous dispersion regime, where high frequencies travel faster than low frequencies. Appendix A provides additional detail on dispersion.

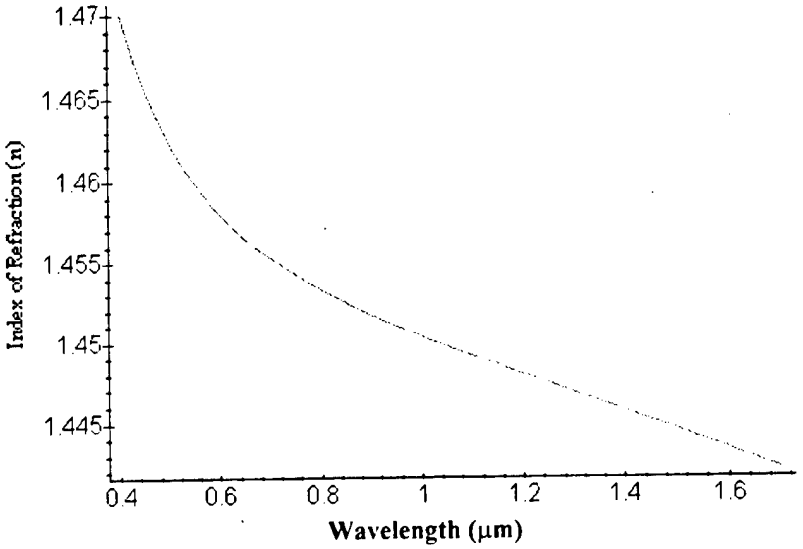

Figure 2.1 Index of refraction profile versus wavelength for bulk fused silica.

The propagation of light in a medium may be quite good, but it is not without loss. Due to numerous loss mechanisms, the optical power measured at the output may be appreciably less than that at the input. With regard to fiberoptics, scattering and absorption comprise the two most significant loss mechanisms. For simplicity, we shall refer to the composite of all loss mechanisms simply as attenuation. Scattering takes the form of *Rayleigh scattering* – inhomogeneities in the material on the order of a fraction of the incident wavelength ($\leq \lambda/10$ or so) act as scattering centers. The attenuation due to Rayleigh scattering is inversely proportional to the fourth power of the wavelength, λ^4, and is generally regarded as the theoretical limit for fiber attenuation. Absorption, on the other hand, is a direct function of specific impurities in the material, most notably the hydroxyl ion, OH^-. Additionally, the creation of lattice vibrations, or phonons, by

photon absorption in the infrared and ultraviolet portions of the spectrum accounts for further attenuation in these regions. (Newport Corporation, 1986)

2. Light in Optical Fibers

The propagation of light within optical fibers is fundamentally no different from electromagnetic radiation propagation through any dielectric media. Optical waveguides, of which fiberoptics is a subset, capitalize on the principle of total internal reflection. Optical rays will traverse the path of least time, i.e. the shortest optical path. Thus, at an interface between materials of differing indices of refraction, an incident ray will obey Snell's Law and bend either toward or away from normal. In the case of optical fibers, the index of refraction of the core is just slightly greater than that of the cladding. For angles of incidence greater than some critical value, denoted by θ_{crit}, all of the energy is contained within the core region due to total internal reflection. In terms of the refractive indices of the core and cladding, the critical angle is given by (Wilson and Hawkes, 1998)

$$\theta_{crit} = \sin^{-1}\left(\frac{n_{cladding}}{n_{core}}\right). \qquad (2.2)$$

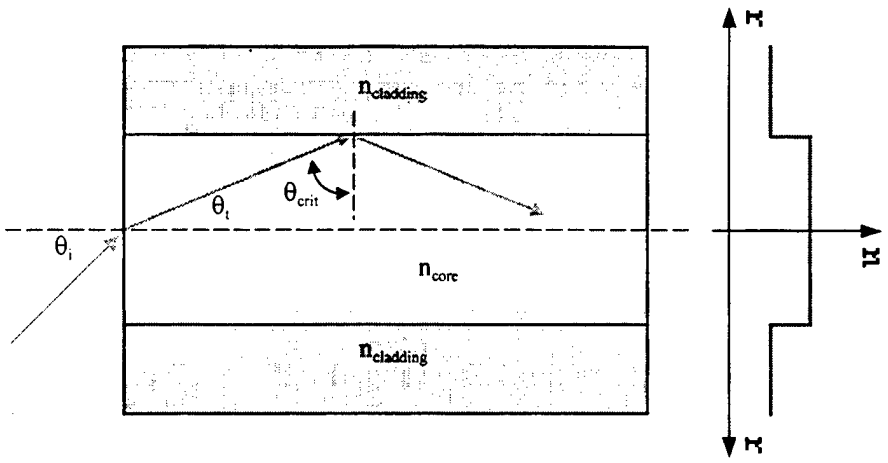

Figure 2.2 Step-index fiber illustrating the difference in indices of refraction between core and cladding. Note the definition of the critical angle, θ_{crit}.

A representative clad fiberoptic cable may possess a critical angle of 80° or more. Figure 2.2 illustrates the refractive index profile of a typical step-index optical fiber.

Inspection of Figure 2.2 shows that only a specific range of values for the incidence angles, θ_i, will propagate down the length of the fiber. This is directly related to the *numerical aperture* (NA) of the fiber. The NA is a measure of the light gathering capability of any optical system, in this case, an optical fiber. Specifically, the NA of an optical fiber takes the form (Newport Corporation, 1986)

$$NA = \sqrt{n_{core}^2 - n_{clad}^2} \,. \tag{2.3}$$

While a NA value of 0.1 to 0.2 is typical of modern fibers, some specially designed fibers may have NAs of 0.3 or higher. The NA of the fiber plays a crucial role in determining which electromagnetic field modes will be supported by the fiber.

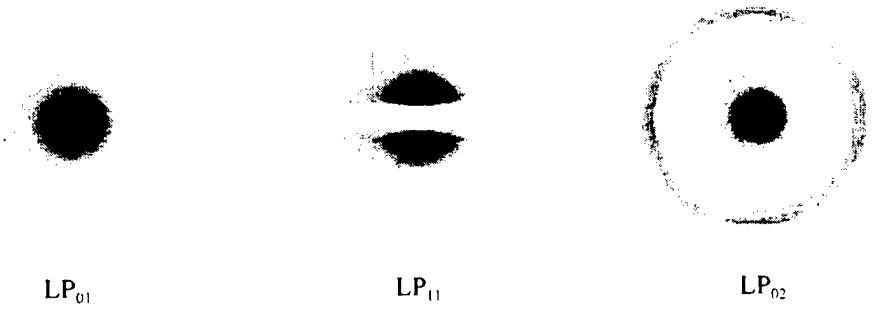

Figure 2.3 Propagation mode patterns and their respective designations for some of the lower order linearly polarized fiber modes.

Figure 2.3 illustrates transmission intensity patterns for three of the lowest order modes supported by a fiberoptic cable of circular cross-section. While they are noticeably dissimilar in appearance, each one represents a valid solution to Maxwell's equations for a circular waveguide. For a fiber such as that depicted in Figure 2.2, the general form of the electric field within the fiber core consists of harmonic Bessel functions that exhibit both temporal and spatial variation. A typical multi-mode fiber

may have hundreds or even thousands of guided modes. In contrast, single-mode fibers can guide only one propagating mode, designated as the HE_{11} mode or fundamental mode. Commonly, the indices of refraction of the core and cladding are within a few percent of each other, and one of three spatial components of the electric field vector will dominate. Thus, the exact solutions can be approximated with a set of simple linearly polarized modes, designated as the LP modes. The LP modes represent combinations of the exact solutions obtained from evaluation of the wave equation. The fundamental mode is denoted as LP_{01} and is shown on the far-left in Figure 2.3. (Newport Corporation, 1986)

The specific modes allowed must be a function of both fiber geometry and composition. The quantity that characterizes these modes is known as the *V-number* of the fiber. The V-number is also referred to as the normalized frequency, characteristic waveguide parameter, or normalized wavenumber and it is given by (Wilson and Hawkes, 1998)

$$V \equiv k_f \, a \, NA \tag{2.4}$$

where k_f is the free space wavenumber defined by $k_f = 2\pi/\lambda_0$, a is the fiber radius and λ_0 is the wavelength in vacuum. The concept of the V-number can be traced back to the eigenvalues, which describe the allowed propagation modes in terms of the 'zeros' of the Bessel functions. For example, the first zero for a Bessel function of zero-order occurs at approximately 2.405. Correspondingly, a fiber with a V-number of less than 2.405 will allow propagation of only the fundamental mode – the HE_{11} or LP_{01} mode. A V-number slightly greater than 2.405 will permit the addition of LP_{11} to the list of permissible modes. This pattern continues as the V-number of the fiber increases (by decreasing the operating wavelength, for example). A V-number exceeding 3.832, the first zero for a Bessel function of first-order, results in the inclusion of the LP_{02} and LP_{21} linearly polarized modes. While a single-mode fiber will always have a V-number of less than

2.405, a representative multi-mode fiber may have a V-number of 100 or more. Thus, it is easy to understand how a multi-mode fiber can support hundreds or even thousands of higher-order propagation modes.

Both, in nonlinear fiber optic applications and in fiber optic communications, single-mode fibers are widely used. A pertinent concept in this regard is that of the *cut-off wavelength*, the wavelength below which the fiber ceases to operate in this single-mode region. Mathematically, this wavelength is determined using Equation (2.4), assuming a V-number of 2.405. For single-mode operation, the operating wavelength must be maintained at a value greater than the cut-off wavelength.

The radial electric field intensity distribution of the fundamental mode can be approximated as a Gaussian of the form (Agrawal, 1995)

$$I(r) = I_0 \exp\left[\frac{-r^2}{w^2}\right] \tag{2.5}$$

where w is a width parameter used for curve-fitting purposes and r is the radial distance from the beam axis.

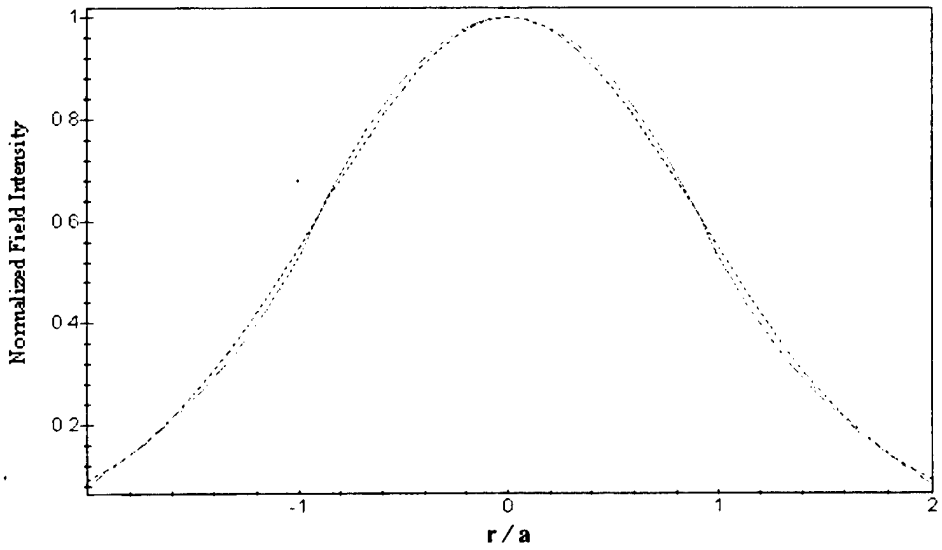

Figure 2.4 Comparison of the exact radial intensity field distribution (solid) versus a Gaussian approximation (dashed) of an optical fiber with a V-number ≅ 2.4.

Figure 2.4 illustrates graphically the normalized intensity distribution of the LP_{01} mode as a function of radial distance from the center of the core. Both curves are for the case where the V-number of the fiber is slightly less than 2.405, the single-mode cut-off point. Although the curves are most closely matched when the V-number is near 2.4, reasonable results are still obtained for values greater than 1.8 or so. Note that the values of +1.0 and –1.0 on the horizontal axis correspond to the points where $|\mathbf{r}| = a$, i.e. the core-cladding interface. We define a quantity known as the mode field diameter to express the spatial width of the Gaussian curve extending out to the $1/e^2$ points. Empirically, the mode field diameter is equal to $2 \times \omega_0$, where (Newport Corporation, 1986)

$$\omega_0 = a(0.65 + 1.619V^{-3/2} + 2.879V^{-6}). \qquad (2.6)$$

Apparent is the fact that the smaller the V-number of the fiber, the broader the resultant electric field distribution will be. In fact, even a fiber with a V-number located at the single-mode cutoff value of 2.405 will exhibit a mode field diameter that is about 10% larger than the core diameter. As a consequence, fibers are typically designed to be operated with a V-number as close to 2.405 as practical. Typical cut-off frequencies are 80 to 90% of the intended operating frequency. For maximum power coupling, the mode field diameters of both the input source and the receiving fiber must be as closely matched as possible. This can be accomplished with either one specialty lens or, perhaps, a series of lenses.

The loss in a fiber can be characterized by an attenuation coefficient, β, which has units of inverse distance. Thus, the power transmitted, P_T, can be expressed in terms of the incident power, P_0, and fiber length, L, as

$$P_T = P_0 \exp(-\beta L). \qquad (2.7)$$

The attenuation coefficient for fibers is typically expressed in dB per kilometer or,

$$\beta_{dB/km} = -\frac{10}{L}\log\left[\frac{P_T}{P_0}\right], \tag{2.8}$$

where L is given in units of kilometers (Agrawal, 1995). The bold red curve shown in Figure 2.5 represents a typical attenuation profile in dB/km for a modern-day optical fiber. Rayleigh scattering dominates at the shorter visible wavelengths while the effects of the hydroxyl ion absorption bands become prominent in the infrared. Owing to the presence of local minima in the attenuation curve at approximately 1.3 and 1.5 μm, the vast majority of modern communication systems are designed for operation at these wavelengths.

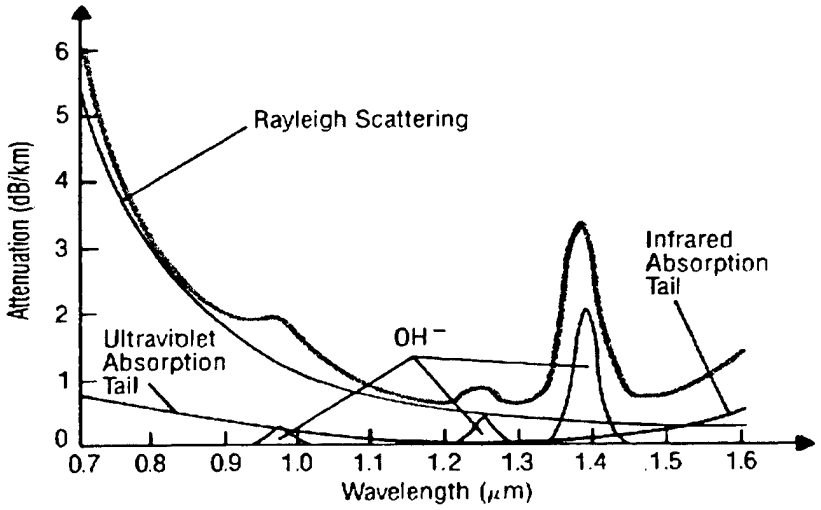

Figure 2.5 Attenuation of an optical fiber as a function of wavelength (Newport Corporation, 1986).

B. NONLINEAR FIBEROPTICS

1. Fundamentals

The response of any dielectric to light is, to first order, linear in character. However, the application of light of sufficient intensity results in a pronounced departure

from linearity. In the case of optical fibers, the origin of the nonlinear response is related to the anharmonic motion of the bound electrons under the influence of an applied electric field (Agrawal, 1995). As a result, the induced polarization **P** of the material is no longer linear with the applied electric field **E**, but rather takes the form

$$\mathbf{P} = \varepsilon_0 \left[\chi^{(1)} \cdot \mathbf{E} + \chi^{(2)} \cdot \mathbf{EE} + \chi^{(3)} \cdot \mathbf{EEE} + \cdots \right], \tag{2.9}$$

where ε_0 is the permittivity of free space and $\chi^{(j)}$ is the electric susceptibility tensor of rank j + 1. The $\chi^{(1)}$ term represents the linear term, and as expected, it is the dominant term in the polarization tensor **P**. Both the material refractive index *n* and attenuation coefficient α are functions of the linear susceptibility. Assuming that the fiber's polarization axis is maintained along its length, for optical fibers operating in the single-mode regime, we can take a scalar behavior for the susceptibility (Agrawal, 1995). In other words, we are assuming that the fiber exhibits negligible birefringence.

All of the nonlinear effects arise as a result of the higher-order terms in the above power series expansion. The $\chi^{(2)}$ term is responsible for difference-frequency or sum-frequency generation, of which second harmonic generation (SHG) is a special case. However, because silicon dioxide (SiO_2) possesses inversion symmetry at the molecular level, $\chi^{(2)}$ vanishes thereby suppressing these second-order effects. Thus, the vast majority of optical fibers do not generally exhibit second-order nonlinearities. The third-order $\chi^{(3)}$ term is the quantity with which we shall be most concerned. It is precisely this susceptibility term that gives rise to, among others, the nonlinear effects of third-harmonic generation, four-wave mixing and nonlinear refraction. As the former two require accurate phase-matching conditions, these processes are generally restricted to specialized crystals and are not prevalent in optical fibers. Thus, most of the nonlinear effects in optical fibers originate from nonlinear refraction.

Consider the simple case of an applied electric field of the form $\mathbf{E} = E_0 \cos \omega t$ such as produced by an electromagnetic wave. Setting $\chi^{(2)} = 0$, assuming a linearly

polarized electric field (for which only one component of the fourth-rank $\chi^{(3)}$ susceptibility tensor is non-zero, namely the $\chi^{(3)}_{xxxx}$ term), and neglecting higher order terms, Equation (2.9) yields

$$P = \varepsilon_0 \left[\chi^{(1)} E_0 \cos \omega t + \chi^{(3)}_{xxxx} E_0^3 \cos^3 \omega t + \cdots \right]. \tag{2.10}$$

Neglecting higher-order terms, Equation (2.10) reduces to

$$P = \varepsilon_0 \left[\chi^{(1)} E_0 \cos \omega t + \chi^{(3)}_{xxxx} E_0^3 \cos^3 \omega t \right]. \tag{2.11}$$

It will be helpful at this point to employ the trigonometry identity

$$\cos^3 \omega t = \frac{3}{4} \cos \omega t + \frac{1}{4} \cos 3\omega t. \tag{2.12}$$

From Equations (2.11) and (2.12), we see that the $\chi^{(3)}$ term lends itself to third-harmonic generation. But, as previously mentioned, this effect is negligible in fiber. Consequently, we shall discard the appropriate term from Equation (2.12) and rewrite Equation (2.11) as

$$P = \varepsilon_0 \overbrace{\left[\chi^{(1)} + \frac{3}{4} \chi^{(3)}_{xxxx} E_0^2 \right]}^{\tilde{\chi}} E_0 \cos \omega t. \tag{2.13}$$

Let us now consider the bracketed terms in Equation (2.13) as being equivalent to an *effective* susceptibility, $\tilde{\chi}$, comprised of both linear and nonlinear terms. Because the refractive index $n = (1 + \chi)^{1/2}$, we can similarly define an *effective* refractive index as

$$\tilde{n} = (1 + \tilde{\chi})^{1/2}, \tag{2.14}$$

or

$$\tilde{n} = (1 + \chi^{(1)})^{1/2} \left[1 + \frac{\frac{3}{4}\chi^{(3)}_{xxxx} E_0^2}{(1 + \chi^{(1)})} \right]^{1/2}. \tag{2.15}$$

As the nonlinear perturbations are typically orders of magnitude less than the linear response, we may expand Equation (2.15) in a power series to yield the desired result of

$$\tilde{n} = n\left(1 + \frac{3}{8} \frac{\chi^{(3)}_{xxxx} E_0^2}{n^2} \right). \tag{2.16}$$

Thus, the refractive index of the fiber is shown to consist of a linear term as well as a nonlinear term as shown in Equation (2.16). Recalling that the index of refraction is fundamentally a function of the optical frequency, we may express Equation (2.16) as

$$\tilde{n}(\omega, |\mathbf{E}|^2) = n(\omega) + n_2 |\mathbf{E}|^2, \tag{2.17}$$

where we define the nonlinear index of refraction, or Kerr coefficient, n_2, as

$$n_2 \equiv \frac{3}{8n} \chi^{(3)}_{xxxx}, \tag{2.18}$$

and the quantity $|\mathbf{E}|^2$ is proportional to the optical intensity within the fiber. It should be noted that the susceptibility component, χ, may be complex. In that case, only the real part is taken.

For a standard telecommunications-grade fiber with an index of refraction, n, of 1.48, the value of n_2 may be on the order of 10^{-16} cm^2 / Watt, a representative value for silica-based fiber. Clearly, significant intensities are required to achieve measurable nonlinear effects. However, by pairing a fiber of relatively small cross-sectional area (i.e. a fiber diameter of less than 5 or 6 μm) with a laser of medium power output (i.e. less than a few Watts), we can fairly easily attain the necessary power densities.

With the continued push for ever higher data rate communications coupled with the availability of inexpensive fiber-based lasers, it is no surprise that the intensity dependent index of refraction is an area of nonlinear optics that has received considerable attention. Two of the better-known effects are self-phase modulation (SPM) and cross-phase modulation (XPM). In both cases, the applied optical field experiences an induced nonlinear phase shift while propagating through the fiber. In the case of SPM, this phase shift is self-induced; for XPM, the phase shift results from interaction with a copropagating field having a different frequency. For the purposes of this investigation, we will concentrate on SPM as it forms the basis for the theoretical operation of the optical loop mirror.

2. Nonlinear Optical Loop Mirror

The basic nonlinear optical loop mirror (NOLM) configuration was first proposed by N. J. Doran and D. Wood in 1988 and is illustrated in Figure 2.6. It consists of a single spool of optical fiber and a fiber coupler (sometimes referred to as an X-coupler) with a power-coupling ratio of $\alpha : 1 - \alpha$. As indicated in the figure, the two output ports are joined via the fiber spool. In this configuration, a single input is split into two counterpropagating fields in the loop. Thus, the optical path length is the same for each field as they traverse identical paths albeit in opposite directions. The two fields then return in coincidence to recombine at the coupler. This design is essentially an all-fiber version of a Sagnac interferometer (Hecht, 1987).

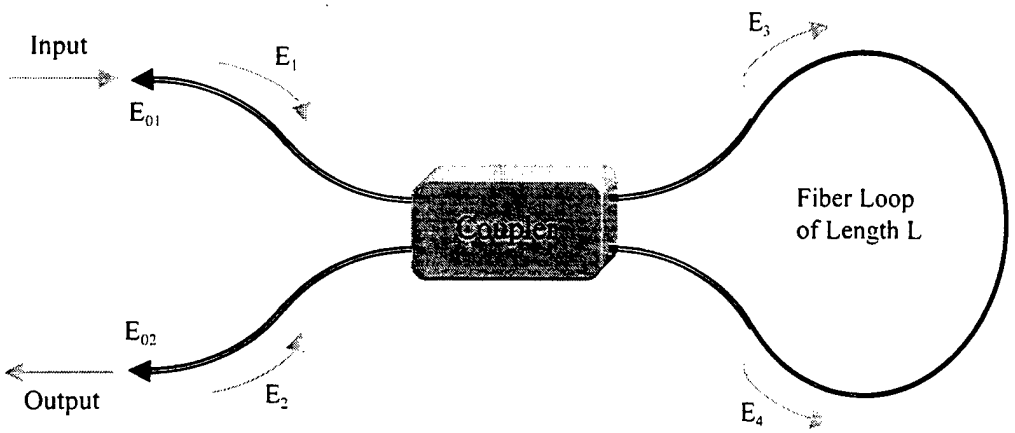

Figure 2.6 Nonlinear optical loop mirror configuration.

The reflectivity, and hence the transmittivity, of a fiber-loop mirror is dependent upon the splitting ratio of the fiber coupler. If the coupler is constructed such that $\alpha = 1 - \alpha$ (i.e. $\alpha = ½$), loop transmittivity will be zero while loop reflectivity will be 100% (hence the use of the term *mirror*). In other words, when $\alpha = ½$, all of the input signal will be reflected back and none will appear at the output regardless of input power level. If, however, the input is not evenly split between the two paths, the propagation of the resulting two fields in the loop will not be symmetric. Due to self-phase modulation (SPM), the phase velocity of each signal is dependent upon its respective intensity. Thus, a nonlinear phase shift will be induced between the two paths due to SPM. Each signal path will similarly undergo a linear phase shift during propagation, but as they are equal, exact cancellation occurs. The net result is that the transmittivity of the NOLM is directly a function of the input intensity. A number of applications have arisen as a direct consequence of this effect. A few examples are optical pulse compression, optical pulse switching, mode locking of lasers and various modulation schemes.

In the following section, we independently derive and verify the theory and detailed operational principles of the NOLM. As anticipated, our final results are identical to those originally introduced by Doran and Wood in 1988.

3. NOLM Theory of Operation

As we saw earlier, the index of refraction, *n*, is a function of both the optical frequency and intensity. Thus, we should expect that the optical path and hence, the phase shift experienced by the fiber upon propagation through a length of fiber will depend upon both items. Thus, the phase of an optical field in a glass fiber changes during propagation according to

$$\varphi = k_0 L \tilde{n} = k_0 L [n(\omega) + n_2 |\mathbf{E}|^2] \tag{2.19}$$

where $k_0 = 2\pi/\lambda_0$ is the free space wavenumber and L is the fiber length. It directly follows from Equation (2.19) that the intensity-dependent nonlinear phase shift can be expressed as

$$\varphi = \frac{2\pi n_2 |\mathbf{E}|^2 L}{\lambda}. \tag{2.20}$$

Assuming a power-coupling ratio of $\alpha : 1 - \alpha$ for the coupler in Figure 2.6, application of input fields of amplitude E_1 and E_2 at ports 1 and 2, respectively, results in output amplitudes E_3 and E_4 as given by (Doran and Wood, 1988)

$$E_3 = \alpha^{1/2} E_1 + i(1-\alpha)^{1/2} E_2 \tag{2.21a}$$

$$E_4 = i(1-\alpha)^{1/2} E_1 + \alpha^{1/2} E_2 . \tag{2.21b}$$

Note the presence of the factor *i* in Equations (2.21) in conjunction with the "$(1 - \alpha)^{1/2}$" terms. Solution of Maxwell's equations inside the ideal coupler requires that the two signal paths possess a fixed differential phase shift between each other. For an idea

coupler, the phase shift is equal to $\pi/2$, hence the factor of i (Gildersleeve, 1997). The presence of the square root in Equations (2.21) is because α is a *power*-coupling ratio.

Consider the simple case of a single input E_{IN} at port 1. As expected, the field will be split via the coupler according to the coupling factor, α. Our goal is to develop an expression for the loop output at port 2 in terms of the input amplitude, E_{IN}. As the fields traverse the fiber loop, each will acquire a phase shift dependent upon its respective intensity. Thus, Equations (2.21) take the form

$$E_3 = \alpha^{1/2} E_{IN} \exp[i\varphi_3] \tag{2.22a}$$

$$E_4 = i(1-\alpha)^{1/2} E_{IN} \exp[i\varphi_4], \tag{2.22b}$$

following appropriate substitution and inclusion of the intensity-dependent phase factors denoted by φ_3 and φ_4. Inspection of Equation (2.20) allows us to rewrite Equations (2.22) in terms of the length of the fiber loop, L, as

$$E_3(L) = \alpha^{1/2} E_{IN} \exp[i\alpha|E_{IN}|^2 2\pi n_2 L/\lambda] \tag{2.23a}$$

$$E_4(L) = i(1-\alpha)^{1/2} E_{IN} \exp[i(1-\alpha)|E_{IN}|^2 2\pi n_2 L/\lambda], \tag{2.23b}$$

where we have substituted the phase factors.

With Equations (2.23) specifying the form of the electric fields within the fiber loop, we now develop equivalent expressions for the output fields at ports 1 and 2 as

$$E_1 = i(1-\alpha)^{1/2} E_3 + \alpha^{1/2} E_4 \tag{2.24a}$$

$$E_2 = \alpha^{1/2} E_3 + i(1-\alpha)^{1/2} E_4, \tag{2.24b}$$

where the explicit dependence on the loop length, L, is understood but has been left off for simplicity. Denoting port 2 as the output port, we can rewrite Equation (2.24b) as

$$E_{OUT} = \alpha^{1/2} E_3 + i(1-\alpha)^{1/2} E_4. \tag{2.25}$$

Now, we combine Equations (2.23) with Equation (2.25) to yield an expression for the output amplitude E_{OUT} in terms of only the input field E_{IN} and the loop parameters, α and L. The expression is as follows:

$$\begin{aligned} E_{OUT} = {} & \alpha E_{IN} \exp[i\alpha |E_{IN}|^2 2\pi n_2 L/\lambda] - \\ & (1-\alpha) E_{IN} \exp[i(1-\alpha)|E_{IN}|^2 2\pi n_2 L/\lambda]. \end{aligned} \tag{2.26}$$

Because we ultimately are concerned with the input and output powers, as opposed to the field amplitudes, we now multiply each side of Equation (2.26) by its complex conjugate. The resultant equation is rather lengthy and after some simplification is given by

$$\begin{aligned} |E_{OUT}|^2 = {} & |E_{IN}|^2 + 2\alpha^2 |E_{IN}|^2 - 2\alpha |E_{IN}|^2 - \\ & \alpha(1-\alpha)|E_{IN}|^2 \times \left\{ \begin{array}{l} \exp[i(1-2\alpha)|E_{IN}|^2 2\pi n_2 L/\lambda] + \\ \exp[-i(1-2\alpha)|E_{IN}|^2 2\pi n_2 L/\lambda] \end{array} \right\}. \end{aligned} \tag{2.27}$$

Grouping terms and applying a simple trigonometry identity allows us to greatly simplify Equation (2.27) and we finally arrive at our desired expression of

$$|E_{02}|^2 = |E_{01}|^2 \left[1 - 2\alpha(1-\alpha)\{1 + \cos[(1-2\alpha)|E_{01}|^2 \times 2\pi n_2 L/\lambda]\}\right], \quad (2.28)$$

where we have adopted the nomenclature used in Figure 2.6 for the input and output fields, E_{01} and E_{02}, respectively.

As expected, if $\alpha = ½$ in Equation (2.28), there is no output at port 2. Rather, the entire signal is reflected back to the input port and we have a perfect mirror. In contrast, for any $\alpha \neq ½$, all of the input power, $|E_{01}|^2$, is transmitted out at port 2 whenever the argument of the cosine function is an odd multiple of π. Put simply, 100% of the power is emitted from the output port whenever

$$(1-2\alpha)|\mathbf{E}|^2 2\pi n_2 L/\lambda = m\pi \quad (2.29)$$

for odd *m*. The minimum output power, which occurs for even multiples of π, is given by

$$|E_{02}|^2 = |E_{01}|^2 [1 - 4\alpha(1-\alpha)]. \quad (2.30)$$

Some limiting conditions exist for Equation (2.28), which should be mentioned. If α equals either 1 or 0, the coupler is essentially transparent and the maximum signal appears at the output. In contrast, if the value of n_2 is zero, there is no nonlinear phase shift incurred in the loop and output power is a minimum; the form is identical to that of Equation (2.30).

Based on the previous discussions, it is apparent from Equation (2.28) that the loop output power varies sinusoidally as a function of the input power (Darwood, 1996). Solving Equation (2.29) for the input power, $|\mathbf{E}|^2$, reveals that the output swings from a

maximum to a minimum every time the input power increases (or decreases) by an amount equal to $\lambda / [2\,(1 - 2\alpha)\,n_2 L]$. Clearly, this amplitude modulation process is a function of a number of parameters – wavelength, coupling ratio, fiber loop length, nonlinear properties of the material and input power. However, once the physical system is constructed and the choice of laser has been made, the only remaining free variable is the input power. Thus, by varying the input amplitude of the NOLM, or equivalently, varying the output power of the laser, we can impress a corresponding amplitude modulation upon the output.

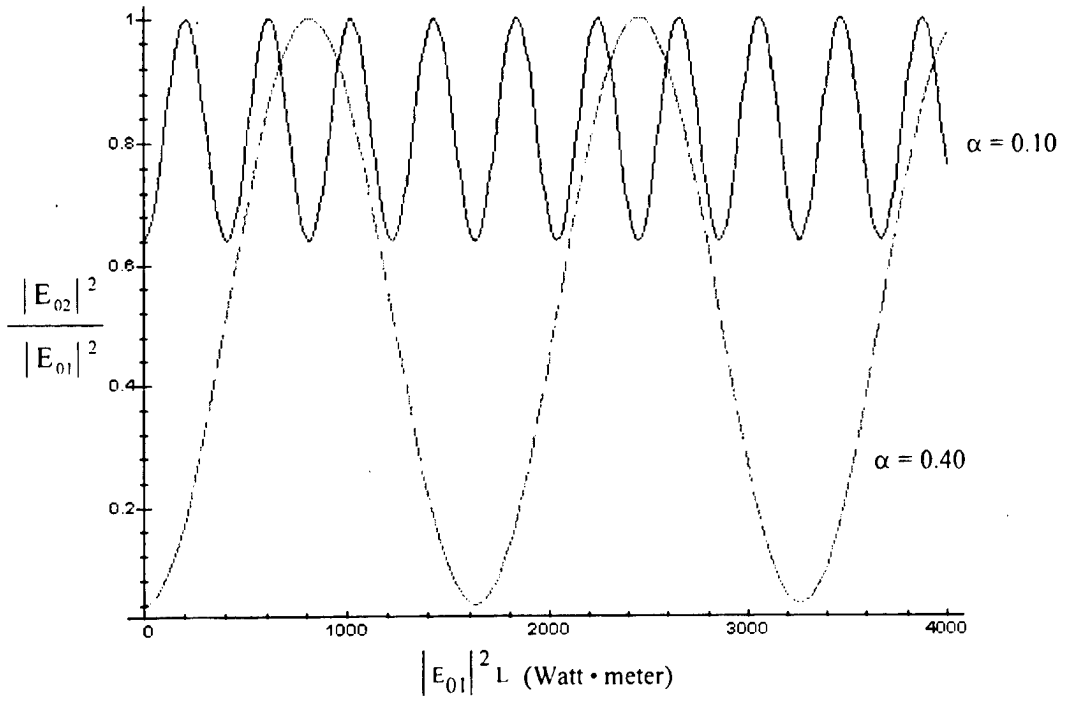

Figure 2.7 NOLM output $|E_{02}|^2 / |E_{01}|^2$ versus the product of input power and loop length for $\alpha = 0.4$ (dashed curve) and $\alpha = 0.1$ (solid curve).

Equations (2.28) through (2.30) show that a value of α closest to 0.5 will provide the greatest degree of modulation (differential between the peaks and valleys of the output); however, this comes at the expense of the need for higher input amplitudes to the fiber loop, and therefore, higher power lasers. On the other hand, a value of α closer to zero reduces the magnitude of output modulation, but the benefit is that the required input power is likewise lessened. Figure 2.7 is a plot of the ratio of the output power to the

input power using Equation (2.28) for two different α coupling factors assuming a wavelength $\lambda = 1.064$ μm, a nonlinear coefficient $n_2 = 3.2 \times 10^{-16}$ cm^2 / W typical for silica-based fiber, and a fiber diameter of $d = 5$ μm. The horizontal axis of the graph is scaled in units of watt-meters to remove explicit reference to the length of the fiber.

Figure 2.8 is another graphical representation of the solution to Equation (2.28). In practice, it is somewhat more useful than Figure 2.7 from an experimentalist viewpoint. In contrast with the previous figure, Figure 2.8 assumes a length of fiber, L, of one (1) kilometer in the analysis. The numerical values of the other variables are identical to that utilized in the previous graph. While Figure 2.7 displays a normalized output (with respect to the input power), Figure 2.8 directly relates the input and output powers of the NOLM in measurable units of Watts. This figure clearly illustrates the trade-off between high and low values of the α coupling ratio.

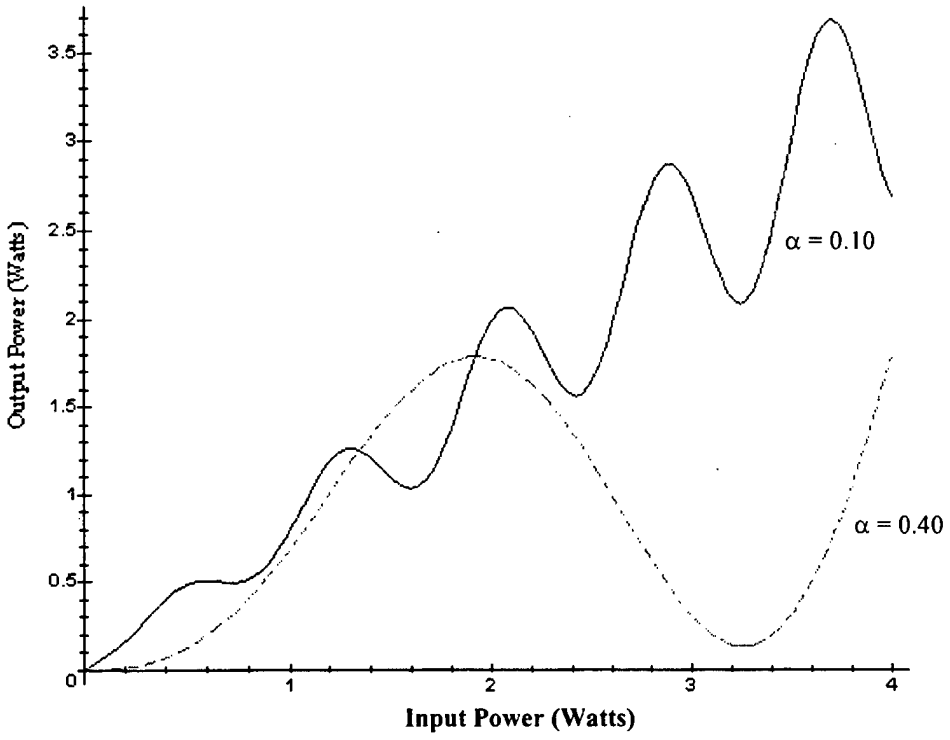

Figure 2.8 NOLM output power versus input power with loop length L = 1.0 km for $\alpha = 0.4$ (dashed curve) and $\alpha = 0.1$ (solid curve).

III. EXPERIMENTAL SETUP AND TEST EQUIPMENT

A. OVERVIEW

To validate the theoretical operation of the nonlinear optical loop mirror (NOLM) as presented in Chapter II, a suitable experiment to demonstrate proof of concept was devised. In this chapter, we discuss both the experimental setup and the array of test equipment necessary for its execution. Specific measurements and test result data will be covered fully in Chapter IV, Experimental Results and Conclusions.

B. LABORATORY EQUIPMENT

1. General Photonics YAG-TWO™ Laser

The laser used in this experiment is a solid-state crystal of yttrium aluminum garnet (YAG) doped with trivalent neodymium (Nd^{3+}) atoms. The 'pump' for the laser is provided by two 1000W tungsten-halogen hybrid lamps mounted in dual-elliptical cavities adjacent to the Nd:YAG crystal. As the lamps generate a tremendous amount of heat, direct water cooling of the crystal is required to prevent thermal stress damage. A closed-loop Korad laser cooler was utilized for this purpose. Because excessive heat generation within the optical cavity tends to result in not only diminished output powers but also beam instabilities, it was crucial to maintain adequate cooling water to the laser during operation.

While there exist several possible output wavelengths for the Nd:YAG laser ranging from 946 nanometer (nm) to 1833 nm, the dominant (and most powerful) line occurs at about 1060 nm, or 1.06 micrometer (μm). Accordingly, the 1.06 μm line was chosen for this experiment. The natural linewidth of the laser is approximately 10 GHz or equivalently, about 0.04 nm, depending on choice of operating wavelength. The laser has the capability to be operated in any one of several modes; for our purposes, the output will be restricted to a single transverse mode designated as the TEM_{00} mode. This will provide us with a beam that has low divergence, optimum stability and a Gaussian

profile. It should be noted that the output of the YAG-TWO™ is unpolarized (i.e. the electric field vector has no preferred spatial orientation). Nominal performance specifications for this mode of operation are

- Output wavelength: 1.064 μm.
- Power output: 2.0 Watts, CW (maximum).
- Beam diameter: 2.0 millimeters (mm).
- Beam divergence: 2.0 milliradians (mrad).

2. Uniphase Model 1101P Helium-Neon Laser

The He-Ne laser is used simply as a tool to aid in the complex process of alignment of the Nd:YAG output beam as well as facilitating the coupling of the beam to the fiberoptic cable itself. As the Nd:YAG's 1.06 μm output wavelength falls in the near infrared (IR) portion of the electromagnetic spectrum, the beam is invisible to the human eye; thus, the utility of the He-Ne laser is readily apparent. The output wavelength of the He-Ne laser is 633 nm, which corresponds to the color red. Minimum output power is 1.0 milliwatt (mW) in the TEM_{00} mode; the output beam is polarized. The beam diameter is 0.63 mm and the beam divergence is 1.3 mrad.

3. New Focus Model 9131 Five-axis Fiber Aligner System

A critical element of the experimental setup is the device that is used to precisely align the free-space laser beam to the bare fiberoptic cable (Figure 3.1). The New Focus Model 9131 incorporates a microscope objective holder and also allows for the use of either bare or 'connectorized' fiber. As opposed to bare fiberoptic cable, connectorized fiber has any one of several types of screw-on or push-on connectors installed at either one or both ends. Additionally, the fiber positioner provides three axes of translation and two axes of rotation to yield resolution on the order of 0.01 μm. For this experiment, single-mode fiber was used exclusively; the core diameters of the chosen fibers ranged

from a minimum of about 2.3 μm to a maximum of 5.0 μm. Clearly with such small dimensions, the highest alignment precision is required.

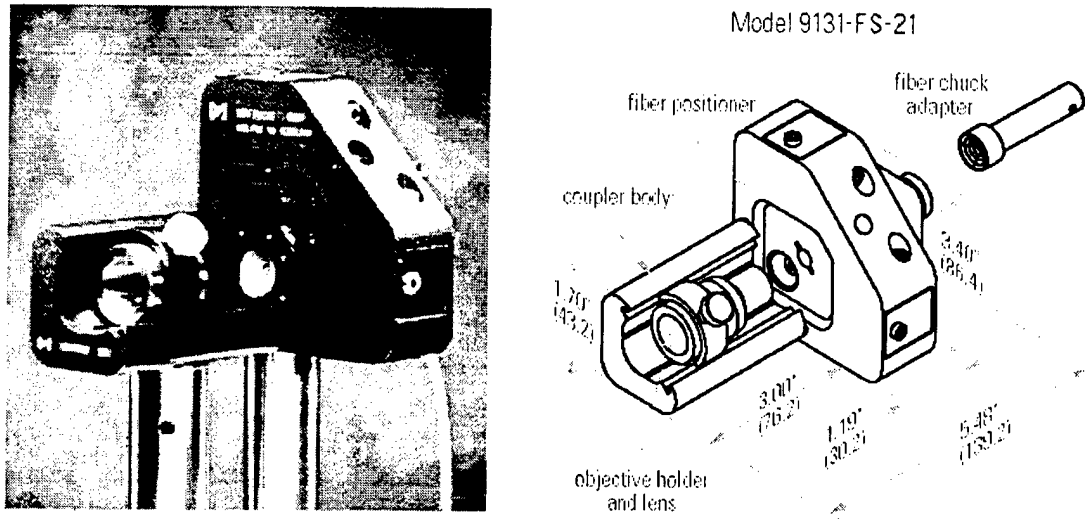

Figure 3.1 New Focus Model 9131 Fiber Aligner photograph and detailed schematic.

4. Coherent Model 205 CW Power Meter

There are two laser power meters used in this experiment, the Model 205 being the primary one. The 205 uses a thermal disc type of detector which utilizes a system of thermocouples to accurately measure the incident radiation over the range of wavelengths from 0.3 to 30 μm. Response time is less than 1 second and accuracy is stated to be ±5% at 10.6 μm.

5. Gould Asymmetric Fiberoptic Couplers

Two fiberoptic couplers, each of which is configured as a two-port by two-port (2 × 2) device, were used in the experiment. While the typical configuration is that of two inputs and two outputs, our experiment modified this setup somewhat (Figure 3.2). Of particular note are the two ports located to the right in the diagram, labeled Output #1 and Output #2, respectively. It is to these two ports that our spools of fiber are to be connected, thereby forming a closed optical path. A signal inserted at the input port is

split into two independent signals, which then exit the coupler via the two output ports on the right hand side. Following a complete (counterpropagating) traversal of the fiber spool, the two signals then reenter the coupler, recombine and exit via the primary output port. A fraction of the signal will likewise exit the coupler via the 'input' port as well; this condition is unavoidable but should in no way compromise the integrity of the results.

Figure 3.2 Asymmetrical fiberoptic coupler illustrating the primary input and output ports. Note that Output ports #1 and #2 serve a dual function (refer to text).

Two different couplers (Figure 3.3) were used in the experiment – one having a 10:90 coupling ratio and the other having a 30:70 ratio. These ratios represent the amount by which the input power is divided between the two output ports. The Gould couplers rely upon the principle of evanescent coupling between the two fiber cores to effect the requisite coupling. Some losses are inevitably induced by the insertion of the

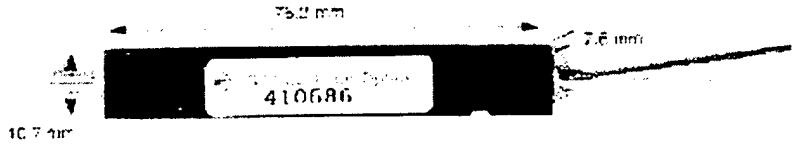

Figure 3.3 Gould 2 × 2 fiberoptic coupler identical to those utilized in this experiment.

coupler into the optical fiber path; factors such as lateral offset and axial and angular separation of the fibers all contribute to degradation in coupling efficiency. Because the two fibers used in the experiment have dissimilar core diameters (2.3 μm and 5 μm), a compromise in the design of the couplers was necessary. The couplers were specified to be constructed using Corning Flexcor™ 780 fiber, which has a core diameter of 4.0 μm.

Although not an optimum situation, the Flexcor™ fiber should provide reasonably good coupling to either the larger or the smaller fiber.

6. The Fiber

Two dissimilar fiber types were used as test platforms in the experiment. Each will be discussed separately below.

a. Corning Flexcor™ 1060

The first of two fiber spools consists of a development fiber produced by the Corning® Photonics Technologies Division. The fiber designation is Flexcor™ 1060 and it is designed to be used in the single-mode operating window of 980 nm to 1060 nm. Thus, it is ideally suited for use with a Nd:YAG laser. The fiber construction is typical – a silica core lightly doped with germanium (to slightly raise its index of refraction) surrounded by a pure silica cladding. The result is a stepped index of refraction profile in the fiber's radial direction (as illustrated in Figure 2.2). The specifications include:

- Maximum attenuation (dB / km)	≤ 1.5 @ 1060 nm
- Cut-off Wavelength (±50 nm)	920 nm
- Mode Field Diameter (±0.5 μm)	6.2 μm @ 1060 nm
- Core Diameter (μm)	5.0 μm
- Cladding Diameter (±2.0 μm)	125.0 μm
- Fiber Length (m)	1000 m (approximate)
- Numerical Aperture (NA)	0.14 (approximate)

Performance tests were conducted on the fiber spool following completion of the connectorization process by the vendor. Total attenuation loss was measured to be 2.0 dB for the entire one-kilometer spool. It should be noted, however, that these test procedures are standardized, and thus were not conducted under optimum conditions for the fiber on hand. All tests were conducted 1) at an operating wavelength of 1550 nm, 2) by coupling

the test fiber to 9/125 (core/cladding diameter) reference standard fiber, and 3) using a full cord test (i.e. reference fibers were mated to both ends of the fiber undergoing test). Clearly, any deviations from the intended operating wavelength as well as mismatches in the mating areas between the two fibers will result in departures from ideal performance.

b. Lucent Technologies Specialty Fiber

This second fiber spool holds great promise for the purposes of this experiment. Manufactured by Lucent Technologies as an experimental fiber, it was designed solely for research purposes. The following specifications were provided: length is about 350 meters; cladding diameter is a nominal 125 μm; core diameter is a very small 2.3 μm; cutoff wavelength is 960 nm; fiber has a stepped index of refraction profile with a Δn equal to 0.033 ($\Delta n \equiv n_{core} - n_{cladding}$). Thus the numerical aperture (NA) is approximately 0.32 and mode field diameter is 2.7 μm when operating at 1060 nm. At first glance, this fiber appears to be constructed very much like the previous one. There is, however, one very significant difference between the two. While the Flexcor™ fiber's core is slightly doped (3 to 4% molar concentration by volume) with germanium to raise its index of refraction, the Lucent fiber has a doping level about seven times larger. Two significant consequences arise as a result. The attenuation loss will be greater, and the fiber nonlinearities will likewise increase. Performance testing identical to that conducted on the Flexcor™ fiber showed an overall loss of 9.3 dB for the 350-meter spool of this highly doped fiber. While many of the loss mechanisms for the two fibers are equivalent, the dissimilar dopant levels apparently lend itself to greater losses in the Lucent fiber.

C. EXPERIMENTAL SETUP

1. The Principles

While, in principle, the setup is rather simple, in practice, the interfacing of the various pieces of equipment proved to be challenging. As indicated in Figures 3.4 and

3.5, the He-Ne laser is used for the purpose of alignment only. As the Nd:YAG output is in the near infrared, and therefore invisible to the human eye, precision optical alignment required the use of the red line of the He-Ne laser. While not shown in Figure 3.5 (for simplicity), the alignment portion of the setup includes a combination of two small planar mirrors oriented at right angles to each other (as shown in Figure 3.4). Acting together, these mirrors allow the He-Ne beam to pass directly into the back of the Nd:YAG laser cavity, through the rear mirror, through the Nd:YAG crystal itself, and then out through the output mirror. This way, by extending the length of the laser 'arm' via the use of mirrors, the overall alignment sensitivity is increased in direct proportion to the length of the arm (cumulative distance measured from He-Ne output to the rear mirror of the Nd:YAG laser).

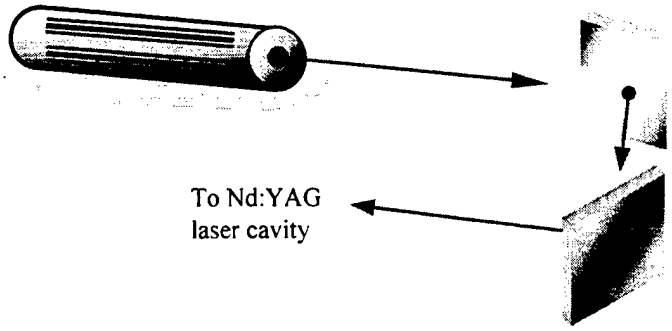

Figure 3.4 Alignment portion of experimental setup using He-Ne gas laser and two-mirror arrangement.

Although utilization of the He-Ne laser is emphasized in the alignment process, one must remember that the ultimate goal of this procedure is to achieve maximum power coupling from the Nd:YAG laser to the fiber. Coupling between the fiber and the He-Ne is both expected and desired in this particular setup; limited coupling to the He-Ne serves as a starting point from which we can then proceed to optimize the coupling efficiency to the Nd:YAG. Accordingly, the physical orientation of the equipment is structured with a deliberate bias in favor of the Nd:YAG laser. Given the contrasting beam characteristics of the He-Ne and the Nd:YAG lasers, it would be exceedingly difficult to optimize the geometries for both.

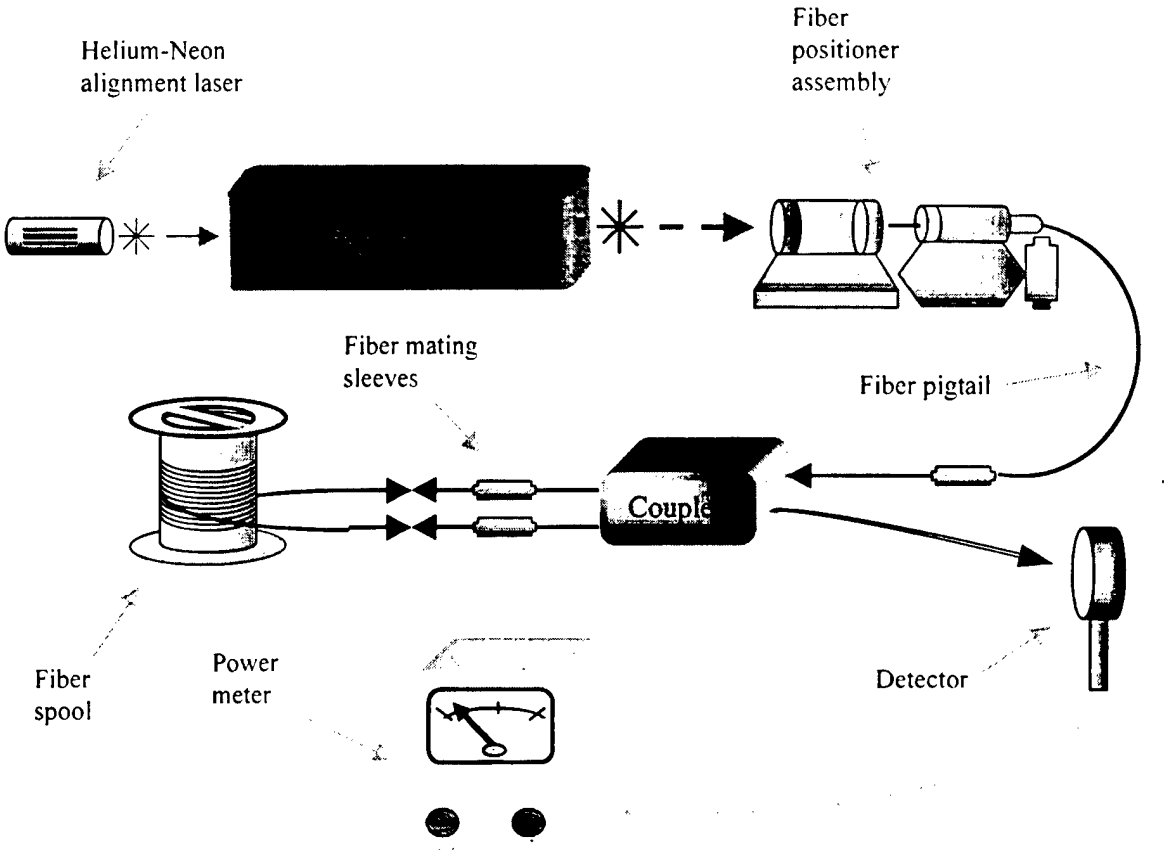

Figure 3.5 Setup for the Nonlinear Optical Loop Mirror experiment. Refer to section B of this chapter for equipment specifics.

The fiber positioner assembly is situated on the optical bench so as to optimize the transfer of power from the Nd:YAG to the core of the fiber. In this case, the fiber to which we are referring is a pigtail (short length of fiber in which one end is connectorized and the other bare) constructed of Corning Flexcor™. The Nd:YAG beam is precisely aligned and focussed to the bare end of the Flexcor™ fiber pigtail via an aspheric objective lens integral to the positioner assembly. Regardless of which of the two fiber spools is used in the experiment, the direct laser to fiber coupling is always accomplished using the Flexcor™ fiber; this precludes having to reposition the positioner assembly when fiber spools are interchanged. To determine the proper placement of the positioner, we rely upon the equations (Newport Corporation, 1986)

$$d_{beam} = d_0 \sqrt{1+\left(\frac{z\theta}{d_0}\right)^2} \qquad (3.1a)$$

$$d_{waist} = \frac{4\lambda_0 f_{objective}}{\pi d_{beam}}, \qquad (3.1b)$$

where the terms are defined as follows: d_{beam} is the diameter of the laser beam at the rear focal plane of the objective lens, d_0 is the diameter of the laser beam at the Nd:YAG output (2.0 mm), θ is the divergence of the Nd:YAG laser beam (2.0 mrad), z is the distance from the Nd:YAG output to the rear focal plane of the objective lens, d_{waist} is the diameter of the waist of the focussed laser beam, $f_{objective}$ is the focal length of the objective lens (10.0 mm), and λ_0 is the wavelength of the Nd:YAG laser (1.064 μm).

For optimum coupling, we require that the diameter of the focussed laser beam, d_{waist}, be equal to the mode field diameter ($\equiv 2 \times \omega_o$) of the fiber. In the case of the Flexcor™ fiber, the mode field diameter is approximately 6.13 mm while the core diameter is only 5.0 mm. Thus, the numerical value for d_{waist} is known. We are left with two equations and two unknowns in Equations (3.1). Solving for the distance from the Nd:YAG laser to the rear focal plane of the objective lens indicates that the optimum span, z, is 47.1 cm, or about 18 ½ inches. Accordingly, the fiber positioner assembly was placed at approximately this distance from the output mirror of the Nd:YAG. It should be apparent from Equations (3.1) that a considerably different answer would have resulted if we instead had opted to maximize coupling to the He-Ne.

2. The Practice

With the various pieces of gear appropriately oriented, we now address the sequence of events required to successfully execute the experimental procedure. It may be helpful to refer to Figure 3.5 in the course of this discussion. Note that the Nd:YAG is

not yet energized. As stated previously, our first order of business is to perform a visual alignment of our optics using the He-Ne laser. Accordingly, we adjust the two alignment mirrors such that the He-Ne beam passes directly through the middle of the Nd:YAG crystal and both cavity mirrors. The importance of this step can not be overemphasized. As closely as possible, we desire that the He-Ne and Nd:YAG beam patterns be concentric.

With the He-Ne beam properly aligned, we now optimize the power transfer from it to the Flexcor™ fiber pigtail through precise manipulation of the fiber positioner assembly. With the fiber pigtail disconnected from the 2 × 2 coupler, we monitor the power output using a meter designed specifically for the He-Ne laser; in this case, we used a Newport Corporation Model 815 digital power meter. Once this output is maximized and excellent coupling of the He-Ne is achieved, we may de-energize this laser for the remainder of the experiment, as it is no longer required. As a point of reference, a worthy goal in the task of coupling the He-Ne laser to the fiber is a total loss (as measured from input to output) of less than 1.0 dB, or about 20%. However, losses of up to 2.0 dB, or about 37%, should still yield satisfactory results. We now turn our attention to the Nd:YAG laser.

After the appropriate safety precautions have been taken, we may now energize the Nd:YAG. If we have done our job properly in all of the preceding steps, we should expect to observe some amount of IR power at the output of the fiber pigtail. While this power may be quite small, the level should be of sufficient magnitude to reasonably measure with the Coherent power meter. The exact value is not significant; the important point to remember is that we require at least some measurable output when using the Nd:YAG. If we find, instead, that we have no output when using the Nd:YAG, we can justifiably conclude that our setup with the He-Ne was flawed in some respect. Thus, we must first rectify the arrangement with the He-Ne before we can proceed further with the use of the Nd:YAG and the crux of the experiment. Let us assume that we do not encounter this situation; we measure somewhere between 50 and 100 mW at the output of the pigtail. This serves as a starting point from which we can begin to optimize the

coupling from the Nd:YAG to the fiber using the fiber positioner assembly. Recall that the geometries required to optimize coupling with the He-Ne and Nd:YAG lasers are quite dissimilar. With patient adjustment of the positioner, we should expect to achieve a coupling efficiency similar to that obtained when using the He-Ne laser. Assuming a 2.0 Watt output from the Nd:YAG, a reasonable output from the pigtail is about 1 ½ Watts. Having achieved these numbers, we can now connect the fiber pigtail to the coupler and direct our efforts on the remainder of the experiment.

Let us trace the path of a bundle of light of intensity I through the apparatus to illustrate the experimental concept. Naturally, the Nd:YAG serves as the source of our electromagnetic radiation. The light is thus emitted via the output mirror of the Nd:YAG laser. From there, light travels through free space to the objective lens of the fiber positioner assembly. With the bare end of the fiber pigtail positioned at the focal point of the lens, the radiation is focussed on the endface to match the mode field diameter of the fiber. Light propagates through the fiber pigtail, through a mating sleeve, and then enters the coupler. At the coupler, the light splits between the two output ports according to the coupling ratio (let us assume that we are using the 30:70 coupler in this case). Accordingly, light of intensity equal to $0.3\times I$ exits the coupler via the 'right' port and light of intensity equal to $0.7\times I$ exits via the 'left' port; the signals then pass through mating sleeves which connect the coupler to the fiber loop. Each beam propagates through the loop in opposite directions, undergoes self-phase modulation and subsequently arrives back at the coupler. Once again, the two signals recombine in the coupler according to the coupling ratio. We record the intensity of light exiting the coupler at the output port. However, due to the nonlinearities introduced in the loop, the output intensity will be neither $0.3\times I$ nor $0.7\times I$. Rather, the output will be a function of the original input intensity coupled to the fiber loop.

D. EQUIPMENT DIFFICULTIES

As in any experimental effort, we should realistically expect that things will not always go exactly as planned. In this case, the bulk of our problems could be traced

directly to the General Photonics YAG-TWO™ Laser. As specified in Chapter II, the Nd:YAG laser is rated for 2.0 Watts CW operation in the TEM_{00} mode. This was confirmed through brief trial runs of the laser in the spring of 1998. However, subsequent operation of the laser in the facility at San José State University showed a marked degradation in performance; the maximum achievable power was approximately 1.55 Watts. As the San José laboratory utilizes an open-loop cooling system, it was hypothesized that variations in cooling water pressure and flow rate could explain the reduced power output. Recall that the normal cooling method for the laser is comprised of the Korad closed-loop system. For the entire six week duration at the remote facility, the Nd:YAG power level remained constant at this degraded level. Upon the return of the laser to the NPS lab facility, a further performance degradation was observed. Total output power had deteriorated to just over 1.0 Watt.

At this point, we began a series of corrective actions intended to restore the 20-year-old laser to a healthier operational state. Each of the two 1000-Watt halogen lamps was replaced, and the cooling system was flushed and refilled with high-resistivity distilled water. Following a complete re-alignment of the laser cavity, an operational test was performed. No noticeable change in output power was detected. The optical elements now came under closer scrutiny. We removed and cleaned both multi-layer dielectric cavity mirrors using a typical optics-cleaning agent, acetone. The output mirror of the Nd:YAG is a meniscus-type mirror identified as being 96% reflective at 1.06 μm; visually, this element appeared to be in excellent condition. In contrast, the rear mirror of the Nd:YAG is of plano-concave design and stipulated to be highly reflective at 1.06 μm; inspection of this mirror under a microscope revealed a slight 'dielectric burn' at the geometric center of the mirror. Without an exact replacement mirror on hand, we substituted a planar mirror having the appropriate dielectric coating. The cavity was transformed from one that was confocal-based to one that was now hemispherical (Wilson and Hawkes, 1998). Again, there was no discernable change in output power. We concluded that the dielectric degradation of the rear mirror contributed little to the overall degradation of the laser system. Thus, the original mirror was re-installed.

With the elimination of the mirrors as a potential source of trouble, we began to look elsewhere. Specifically, we analyzed the pumping enclosure, the dual-elliptical cavity housing both pump lamps. The cavity, itself, is cast of heavy bronze and then gold-plated. Removal of the lamps allowed us to polish the gold coating using soft lint-free lens tissue. As this resulted in no performance gains, we experimented with slight changes in the physical orientation of the lamps (although it is only a small amount, the lamps can be raised or lowered with respect to the cavity). Once more, no change was observed. We began to consider the possibility that the problem could be completely unrelated to the optics of the laser and that an electrical fault may be the culprit. Subsequent measurements of the voltage output at some essential points in the laser control circuitry quickly dispelled that theory, however. Meanwhile, the laser output continued on its gradual degradation slope. Output power was now in the vicinity of ½ Watt. None of our well-intentioned corrective actions had achieved even the slightest increase in power output. More extreme measures were clearly required.

As only a few troubleshooting avenues remained open to us, we decided to completely disassemble the pumping enclosure, remove the solid-state neodymium crystal (laser rod) and inspect it for damage. Although one end-face of the rod possessed a decent coating, the other side appeared to have none. Inspection of the pumping enclosure revealed a small dried water spot indicative of a very slow cooling water leak toward the side of the rod without the coating. Perhaps a small quantity of water had seeped onto the rod end-face during operation resulting in intense heat generation and eventual failure of the dielectric coating. Fortunately, we were able to located a Nd:YAG rod of similar dimension at a neighboring lab facility. Installation of the 'new' rod, however, resulted in the Nd:YAG's complete inability to lase. Out came the loaner rod. Subsequent comparative analysis of the two rods revealed significant design differences between the two. The loaner rod was found to be configured with planar end-faces each canted at 1° and oriented parallel to each other. The original rod was quite unlike this as we eventually determined. Because General Photonics is no longer in business and the operator's manual provides little in the way of technical information, we performed a

series of tests to quantify the specifications on the laser rod. One end-face was planar and oriented perpendicular (0°) to the axis of the rod; the other end-face displayed a short (5.0 cm) convex radius of curvature. Hence, the rods were far from interchangeable.

All fingers continued to point to the rod as the source of our problems. Armed with the design specifications, we could now elicit some professional repair assistance. The rod was soon in the mail to a facility to re-polish and re-coat the end-faces. We had decided to replace the rear cavity mirror as well. Similar tests to those performed on the laser rod were performed on the mirror to determine its exact radius of curvature. A match was found, but the diameter of the replacement mirror was too large for the tilt-stage mount of the laser. Another repair facility was tasked with grinding the existing mirror to the desired dimensions. Both repairs were executed extremely well and the components were installed back into the laser in the early part of December 1998. A complete realignment of the cavity was performed and the output power was measured. The resultant power readings were lower than they had ever been previously. Maximum output power remains between 100 and 150 mW. Time constraints prohibit us from embarking on any further troubleshooting or repair efforts in the context of this particular investigation.

IV. CONCLUSIONS AND FUTURE WORK

As stated in the final section of Chapter III, chronic equipmental difficulties prevented us from successfully carrying out the experiment as it had been originally conceived. While a substantial amount of time was spent actively pursuing the ultimate goals of this investigation, the majority was spent in troubleshooting and repair efforts.

Although we failed to rectify the problems with the Nd:YAG laser, continuation of this experimental investigation still holds great promise for the future. It is only a matter of time (and effort) until someone breaks the code for the repair of the Nd:YAG. Perhaps the reflectivity wavelength peak of the output mirror has simply shifted from 1.06 μm. Or, the output mirror reflectivity has degraded from the 96% design specification. Or, perhaps the laser rod has developed indiscernible micro-cracks due to repeated thermal cycling. These are just a few possibilities, which may be explored in the context of future thesis work.

The concept of the NOLM remains just as pertinent today as it was when it was first introduced in 1988. In fact, it is probably even more critical now as evidenced by the tremendous growth of the fiberoptic industry. One could conceive of any number of fascinating follow-on experiments based on the NOLM. A quick literary search will reveal a multitude of public and private research facilities currently working on variants of the NOLM. Looking out a few years, a logical evolution of the nonlinear fiberoptics experiments would be the incorporation of a pulsed or Q-switched Nd:YAG laser, preferably diode-pumped and air-cooled. However, for now, a worthy goal is simply the restoration of the General Photonics laser to operational status. As the other necessary research materials are already available, this would serve well as a starting point for future thesis work in nonlinear fiberoptics.

LIST OF REFERENCES

Agrawal, Govind P., *Nonlinear Fiber Optics, 2nd Ed.*, Sections 1.2 – 1.3, 2.2 – 2.3, 3.1, 4.1, 4.4, Academic Press, 1995.

J. W. Darwood, *Non-electro-optic Methods of High Frequency Laser Modulation*, Thesis for Master's Degree Naval Postgraduate School Monterey CA, 1996.

N. J. Doran and D. Wood, *Nonlinear-optical loop mirror*, Optics Letters, Vol. 13, No. 1, pp. 56 - 58, January 1988.

J. S. Gildersleeve, *The Mach-Zehnder Coupler*, Thesis for Master's Degree Naval Postgraduate School Monterey CA, 1997.

Hecht, Eugene, *Optics, 2nd Ed.*, Sections 3.5, 4.3.4, 9.4.2, Addison-Wesley Publishing Company, 1987.

Newport Corporation, *Projects in Fiber Optics, Applications Handbook*, Sections 0.2 – 0.4, 3.1 – 3.3, 3.6, 4.1, 1986.

John Wilson and John Hawkes, *Optoelectronics, an Introduction, 3rd Ed.*, Sections 3.10, 5.5, 8.1 – 8.3, 9.3.1, Prentice Hall Europe, 1998.

APPENDIX A. GROUP VELOCITY DISPERSION

In Chapter II, we introduced chromatic dispersion, the principle defining the process by which the propagation speed of light in a fiber is a function of its frequency. In the study of fiberoptics, both dispersive effects and nonlinearity may or may not play a significant role depending on the specific parameters of the experiment. For example, in the communications field, the presence of pulse broadening due to dispersion will ultimately limit the maximum achievable data rates unless other measures are taken. For this particular investigation, we must consider the effect, if any, of group velocity dispersion (GVD) on our efforts. A little background on GVD may be helpful in this context.

As we know, a pulse will propagate through a fiber at one particular speed, depending upon the material's refractive index profile and the signal frequency. However, unless the pulse is an idealized mathematical construct, it will contain a finite spread, or group, of frequencies. We refer to this propagation speed as the group velocity, v_g, of the pulse. Thus, since each pulse will possess a range of spectral components, individual elements may travel either slower or faster than the pulse envelope as a whole. The net result is a temporal broadening of the pulse over the length of the fiber. The parameter that characterizes this behavior is known as the group-velocity dispersion parameter, β_2. In the normal dispersion regime, β_2 is positive while in the anomalous dispersion regime, it is has a negative value. Mathematically, the dispersion parameter is approximated as

$$\beta_2 \cong \frac{\lambda^3}{2\pi c^2}\frac{d^2 n}{d\lambda^2} \,. \qquad \text{(A.1)}$$

Frequently, a dispersion parameter denoted as D is used in place of β_2 in fiberoptic literature. The relation between the two quantities is expressed as (Agrawal, p. 10)

$$D = -\frac{2\pi c}{\lambda^2}\beta_2 \cong -\frac{\lambda}{c}\frac{d^2 n}{d\lambda^2}. \qquad (A.2)$$

From a practical standpoint, the parameter D is far more intuitive than β_2. The typical units of D are picoseconds per kilometer per nanometer (i.e. ps/km · nm). Thus, the value of D indicates the pulse spread per unit length per unit wavelength interval for a fiber (Wilson and Hawkes, p. 440). Figure A.1 is a graph of the dispersion parameter D versus wavelength for silica fiber using the refractive index profile introduced in Chapter II, Figure 2.1. As opposed to β_2, D is negative in the normal dispersion regime and positive in the anomalous regime. The only significance to the sign of D is to indicate which components of the pulse arrive first, those of lower or higher frequency.

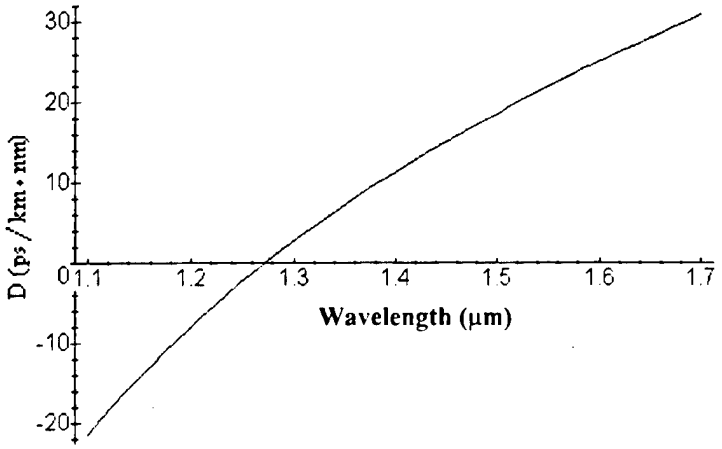

Figure A.1 Dispersion parameter D versus wavelength for bulk fused silica. Note that the zero-dispersion wavelength (λ_D) falls just below 1.3 μm.

The remaining question to be addressed is whether the effects of GVD must be accounted for in this investigation. We know that as pulses become shorter in the time domain, there is a corresponding spread in the frequency domain. In other words, shorter pulses contain a greater number of Fourier components. Conversely, temporally wider pulses will contain few Fourier components. Therefore, with all else being equal, longer pulses will experience less broadening, or dispersion than shorter ones. With 'long' pulses of sufficient optical power, nonlinear effects will far overshadow those of GVD.

Specifically, GVD effects are negligible for relatively wide pulses ($T_0 > 100$ ps) with a large peak power ($P_0 \geq 1$ W) (Agrawal, p. 90). Given that we are operating with a CW laser, GVD can be disregarded for the purposes of this analysis.

INITIAL DISTRIBUTION LIST

1. Defense Technical Information Center 2
   8725 John J. Kingman Rd., Suite 0944
   Ft. Belvoir, VA 22060-6218

2. Dudley Knox Library 2
   Naval Postgraduate School
   411 Dyer Rd.
   Monterey, CA 93943-5101

3. Professor William B. Maier II, Code PH/Mw 1
   Chairman, Department of Physics
   Naval Postgraduate School
   Monterey, CA 93943-5002

4. Professor Andrés Larraza, Code PH/La 2
   Department of Physics
   Naval Postgraduate School
   Monterey, CA 93943-5002

5. Professor H. Sarma Lakkaraju 2
   Department of Physics
   San José State University
   San José, CA 95192-0106

6. Frederic Quan 1
   Corning Incorporated
   Sullivan Park FR-2
   Corning, NY 14831

7. David J. DiGiovanni 1
   Lucent Technologies
   700 Mountain Avenue
   Murray Hill, NJ 07974-2070

8. LT David S. Grennek 2
   419 East Edgewood Avenue
   New Castle, PA 16105